Stony Brook University

OFFICIAL COPY

The official electronic file of this thesis or dissertation is maintained by the University Libraries on behalf of The Graduate School at Stony Brook University.

© All Rights Reserved by Author.

Development of a single photon detector for fluorescent spectrometry

A Thesis Presented

by

Dmytro Gudkov

to

The Graduate School

in Partial Fulfillment of the

Requirements

for the Degree of

Master of Science

in

Electrical Engineering

Stony Brook University

December 2011

Stony Brook University

The Graduate School

Dmytro Gudkov

We, the thesis committee for the above candidate for the

Master of Science degree, hereby recommend

acceptance of this thesis.

Vera Gorfinkel – Dissertation Advisor

Associate Professor, Department of Electrical and Computer Engineering

Dmitri Donetski

Assistant Professor, Department of Electrical and Computer Engineering

This thesis is accepted by the Graduate School

Lawrence Martin
Dean of the Graduate School

Abstract of the Thesis

Development of a single photon detector for fluorescent spectrometry.

by

Dmytro Gudkov

Master of Science

in

Electrical Engineering

Stony Brook University

2011

I present a novel single photon spectrometer and discuss its use for ultra-fast and highly accurate detection of quantum dots and micro-beads encoded with compositions of various types of quantum dots.

The spectrometer receives a polychromatic light through a fiber input. The received light undergoes color decomposition by a diffraction grating and is further detected by a 32-channel PMT (Hamamatsu, Japan) operating in single photon counting mode. Due to a novel, highly advanced analog/digital circuitry operating in GHz range, the 32-channel single photon detector has a unique performance: it supports detection of up to 10^8 photon/s/channel, data acquisition rate at up to 10^6 frames/s, data transfer and via Ethernet, and data recording speed up to 32MB/s using a standard PC.

Due to an extremely broad linearity range and high data acquisition speed, the developed spectrometer has been successfully used for the detection of fluorescent radiation from both single quantum dots and micro-beads with embedded quantum dots of different colors. Our experiments demonstrated the ability of the spectrometer to detect up to 10,000 micro-particles per second. For the beads with embedded quantum dots of 6 different colors we were able to

distinguish up to 10^5 different color combinations (QDs fluoresce in spectral range between 490nm and 700nm).

Currently, in the field of molecular biology there is a wide variety of techniques and assays based on color labeled micro- and nano-particles. The unique detection performance of our single photon spectrometer suggests its successful use in multiple applications such as life sciences, molecular diagnostics, personalized medicine and others.

TABLE OF CONTENTS

LIST OF FIGURES

LIST OF TABLES

LIST OF ABBREVIATIONS

Abbreviation or Symbol	Term
APD	Avalanche Photodiode
CE	Capillary Electrophoresis
DC	Dark Counts
OD	Optical Density
PCB	Printed Circuit Board
PCR	Polymerase Chain Reaction
PMT	Photomultiplier Tube
SiPM	Silicon Photomultiplier
SPAD	Single Photon Avalanche Diode

CHAPTER 1

TEORY OF QUANTUM PARTICLES DETECTION IN FLUORESCENCE SPECTROMETRY

1.1 Technology overview.

Over the years fluorescence spectrometry had become one of the primary methods of analysis in biochemistry and biophysics. Its high sensitivity and relative ease of use comparing to radioactive tracers method have brought it a widespread attention and appreciation in many life sciences applications.

Many different technologies have been developed to detect weak fluorescent signals while techniques relying on putting special fluorescent markers on microparticles carrying test substances have become more and more popular in the field of molecular diagnostics because of their simplicity, high sensitivity and specificity, and economic performance.

Recently a number of technologies have been developed for optical “bar coding” of micro objects (beads, cells, etc.) with nano particles. This includes the use of segmented nanorods [1], rare-earth doped glass [2], fluorescent silica colloids [3], photobleached patterns [4], enhanced Raman nanoparticles [5] and semiconductor quantum dots (QD) [6].

While each of the above technologies has its advantages and limitations, luminescent QDs exhibit nearly ideal properties for optical bar coding. Indeed, QDs’ fluorescence emission wavelengths can be tuned continuously by changing the QD size, and a single short-wavelength excitation source can be simultaneously used for exciting multiple colors. High-quality semiconductor-based QDs have relatively narrow and symmetrical emission spectra and are also stable against photobleaching [7]. In principle, at the present state of technology combinations of multiple QD colors and intensities can be used to encode billions of micro objects. However,

practical solution for fast detection and decoding of billions of distinct color codes is an engineering challenge.

In this thesis we will describe a novel instrument - single photon spectrometer – which allows an extremely fast, highly sensitive and accurate detection and recognition of QD-barcoded objects. We shall also present a method which enables an accurate separation of fluorescent signals emitted by individual components of the QD mixes. The linearity dynamic range of the detector's channels exceeds 10^7 photocounts per second and can be enhanced by a factor of 10 with the proposed signal processing algorithms.

1.2 Encoded multicolor particles detection.

Multiplex technologies which allow multiple discrete assays to be performed simultaneously within the same microvolume sample are promising tools in the field of molecular biology and medicine. Multiplex assays typically include screening chemical libraries for compounds of interest and screening for particular target molecules, such as antigens, antibodies, nucleotides and peptides, in test samples. The thousands of individual reactions that are required for these purposes are preferably carried out all at the same time.

One of the most important challenges in developing multiplex assays is the necessity to track each reaction. There are two main approached to do this. In the first approach, each reaction is physically separated — as it is done in 'high-density' DNA arrays or microchips. In the second strategy, the reactions are carried out on individual microcarriers — each carrier having a particular molecule bound to its surface. In the first approach, the identification of the molecule that is analyzed is determined by the exact location on the microarray. The second approach requires each of the microcarriers to be labeled to allow the identification of molecules bound to their surface. This method allows uniquely encoded microcarriers to be mixed and subjected to an assay simultaneously.

Currently, there are four major groups of methods used for encoding microcarriers: optical, electronic, graphical and physical encoding. The most important characteristics for any encoding

method include the number of microcarriers that can be uniquely encoded, size of the microcarrier, and the ability to rapidly and automatically encode and decode the microcarriers. These parameters, in conjunction with the cost of the techniques, determine which encoding strategy will be broadly used for commercial applications.

The electronic encoding methods are based on the use of radio frequency memory tags. An encoded microcarrier comprises a microelectronic chip with an embedded non-volatile unique digital code. When the microcarrier passes a detection zone, the microchip gets activated (electronically or optically) and transmits its ID code as an rf signal. Typical 40-bit code can provide $\sim 10^{12}$ unique ID combinations. Major disadvantage of the electronic encoding is relatively large size of microcarriers ranging from millimeters to hundred microns.

The graphical encoding [1] is based on storing information by spatial modulation of a material of the microcarrier or its properties. Among many graphical encoding techniques, the most promising are graphical-encoded metal particles. The metal cylindrical rods consist of adjacent (submicron) stripes of alternating metals. The minimal useful stripe length is determined by the optical detection resolution, and is estimated to be ~500 nm. The diameter of the rods is between 15 nm and 12 mm, and the overall length of the particles will be between 1 and 50 mm. The number of uniquely encoded rods is virtually unlimited, since many parameters can be varied. The detection can be automated by sending the particles through a cytometer-like system. However, all particles produced in the same process will have identical codes because they were created by the same electrochemical reduction steps (~30min per step). So, to create one million different codes, the process must be repeated one million times.

In optical encoding method, microcarriers can be identified by their absorption or emission spectra as well as by the fluorescence decay time.

In one of the most developed color encoding strategy, the optical codes are created by incorporating distinct proportions of different fluorescent dyes. The ideal dyes should have both coinciding excitation spectra and clearly separated emission bands. Nevertheless, even with the relatively limited degree of multiplexing, the technique has proved to be of great use in many applications, including genotyping, measuring cytokine cadmium and thyroid levels, cystic-

fibrosis screening, genetic human lymphocyte antigen (HLA) typing, kinase testing and allergy testing.

Many of the problems related to organic dyes are largely overcome by using fluorescent semiconductor quantum dots (QD) [7]. Conventional dye molecules have a narrow excitation spectrum, which makes simultaneous excitation of different dyes difficult, and their broad emission spectrum with a long tail at red wavelengths introduces spectral crosstalk between different detection channels. This makes quantification of the relative amounts of different dyes difficult. By contrast, semiconductor QDs have a continuous excitation spectrum, and an emission spectrum that can be continuously tuned by changing the particle size. Their emission spectrum is very narrow (typically 20–30 nm). Therefore, many sizes of QDs can be excited simultaneously with only one wavelength of light, resulting in many emission colors with minimal spectral overlap. Moreover, the quantum dots are more photochemically stable in comparison to conventional fluorophores [7].

However, until recently, brightness and uniformity of encoding signals did not allow identification of microcarriers at high speeds and high accuracies. The breakthrough in this field was made with an advent of a new generation of mesoporous polystyrene beads encoded with surfactant-coated (hydrophobic) quantum dots Prepared by a multiple-stage polymerization process, this class of porous beads is highly uniform in size and contains an extensive network of nanometer-sized pores. These “mesoscopic” pores allow rapid uptake and immobilization of quantum dots through strong hydrophobic interactions between the pore walls and the QD capping ligands (tri-n-octylphosphine oxide, TOPO) [8]. These beads may contain up to several million quantum dots and produce very bright fluorescence (2x104 photons per mW per second per 1 quantum dot).

We would like to emphasize that although at the present state of QD technology billions of distinct color codes can be realized (*9 QD types at 10 intensity gradations would yield 10^9 color codes*), commercially available sets of beads now contain maximum up to hundred distinct codes. Several reasons limit the number of codes including spectral overlapping, fluorescence-intensity variations and signal-to-noise requirements.

In conclusion, in terms of the number of codes, the graphical and electronic encoding strategies are the most promising. Optical encoding strategies, on the other hand, have the advantage of being easier to fabricate, encode and decode microcarriers, since only the overall optical properties of the particles need to be detected.

1.3 Processing of fluorescence spectra.

The main task of the signal processing is the determination of concentrations of individual fluorescent dyes in dye mixtures composed of *n* dyes having distinct and known fluorescent spectra. The concentrations of individual dyes in the mixture can be found by a decomposition of the fluorescence measured in *N* independent channels of the spectrometer, provided the spectrometer produces linear response to the detected fluorescence.

Let us assume that the number of the analyzed fluorescent dyes $n \le N$ (e.g. n=4 for DNA sequencing). Let us introduce the system matrix $\mathbf{H}_{(N\times n)} = (\mathbf{h}_1, \mathbf{h}_2, ..., \mathbf{h}_n)$ where $\mathbf{h}_i = (h_{1i} \ \ldots \ h_{Ni})^T$, $(1 \le i \le n)$ are N-component vectors representing spectra of the fluorescent dyes in the analyzed dye mixture. In order to obtain a system matrix **H** one has to perform the system calibration and measure in advance spectral responses of individual fluorescent dyes $\mathbf{h_i}$. If $\mathbf{r} = (r_1 \ \ldots \ r_N)^T$ is the measured fluorescent spectrum of the dye mixture, and $\mathbf{s} = (s_1, s_2, ..., s_n)^T$ is a vector of component weights representing concentrations of individual fluorescent dyes, than in the presence of noise $\boldsymbol{\omega} = (\omega_1 \ \ldots \ \omega_N)^T$ the measured spectrum

$$\mathbf{r} = \mathbf{H}\mathbf{s} + \boldsymbol{\omega} . \quad (1)$$

The optimal solution **s** of the Eq. (1) depends on the assumption regarding the distribution properties of the noise components ω_i. Simplified assumption about ω_i being

independent identically distributed normal random values yields well known and computationally efficient minimum variance unbiased solution for estimate $\hat{\mathbf{s}}$:

$$\hat{\mathbf{s}} = \left(\mathbf{H}^T\mathbf{H}\right)^{-1}\mathbf{H}^T\mathbf{r}. \quad (2)$$

In photon counting, individual rate observations r_i have Poisson distribution with equal mean and variance. For higher photocount rates (over 50 counts per observation period), the observed rates are well approximated by superposition of 'true' mean rate $\overline{r}_i$ and Gaussian noise ω_i with variance depending on the mean rate:

$$r_i = \overline{r}_i + \omega_i, \quad \omega_i \sim N\left(0, f\left(\overline{r}_i\right)\right).$$

Thus, more precise solution can be obtained by assuming the components ω_i independent non-identically distributed normal random variables. The general solution for Eq.(1):

$$\hat{\mathbf{s}}^* = \left(\mathbf{H}^T\mathbf{C}^{-1}\mathbf{H}\right)^{-1}\mathbf{H}^T\mathbf{C}^{-1}\mathbf{r}, \quad (3)$$

where $\mathbf{C}$ is the covariance matrix of components ω_i. Due to independence of ω_i the matrix $\mathbf{C}$ is diagonal:

$$\mathbf{C} = \begin{pmatrix} \sigma_1^2 & & & 0 \\ & \sigma_2^2 & & \\ & & \ddots & \\ 0 & & & \sigma_N^2 \end{pmatrix}, \quad (4)$$

where σ_i^2 is the variance of ω_i. In practice, mean rate $\overline{r}_i$ is unknown and observed rate r_i is used for the computation of the variance:

$$\overline{r}_i \approx r_i.$$

Variances σ_i^2 are estimated for each measurement. The function that relates σ_i^2 and r_i is specific for each preprocessing method used to obtain r_i. For example, if r_i are obtained directly by counting of photons during a sampling period, then $\sigma_i^2 = r_i$. If background b_i is subtracted from the result of the counting observation, then $\sigma_i^2 = r_i + b_i$. If r_i is obtained by averaging

counting observation over k sampling periods, then $\sigma_i^2 = r_i / k$. The estimator (3) is more accurate, but requires more computational resources than the estimator (2).

The approach described above allows construction of the procedure, which performs background subtraction at the stage of cross-talk removal. This is achieved by creating additional spectrum (column in matrix $\mathbf{H}$) that represents the background. The estimators (2) and (3) with new matrix $\mathbf{H}$ will separate the background from the other spectral components.

Detailed description of the technique and application results can be found in [10].

1.4. Single photon detectors for laser-induced fluorescence.

Fluorescence represents a very low light, of about femtowatts intensity. But, at the same time laser excitation power lies in range of miliwatt. A huge dynamic range detector would be required to cover all possible fluorescence levels.

The power of one picowatt is equal to a photon flux of ~10^7 photons per second. So if the response time of the photon detector to each incoming photon is much less than 10^{-7} second, the detector will see the photon flux as discrete particles. Responding to each single photon, the detector gives an output pulse with amplitude that depends on the internal gain of the detector. Main characteristic of a photon detector is its signal to noise ratio as depending on it a photon event is created. As we can't affect signal intensity, getting the lest noisy detection system is an ultimate goal. Absolute minimum noise of photon detection systems is defined by the Poisson fluctuation due to the stochastic process of avalanche multiplication. Single photon detectors are approaching this lower limit.

There're a number of key criteria a single photon counting detector should satisfy:

- Lowest possible dark count noise.
- Fast response time, to be able to recover after processing one photon event for the next one.

- Large linear dynamic range, to be able to register events of different light magnitude while having a predictable response.
- Spectral range covering large part of 400-1000nm scale, which is typical wavelengths of signals in microbiology applications.
- High sensitivity to the photon events, typically governed by quantum efficiency of the detector.
- Large active area, to overcome coupling losses.
- Multiple parallel channels to be able to register different events happening simultaneously or to provide high spectral resolution in case of multichannel spectrometer.

The subject of this thesis is to describe PMT-based single photon spectrometer having exceptional performance characteristics majorly in counting rate and dynamic range.

1.5 Brief comparison of single photon detectors.

Widely available single photon detectors include PMTs, SPADs and SiPM. While SiPMs are gaining popularity in recent years as a very cheap and potentially efficient photon detectors their relative small detection area and complications with high dark noise still allow PMT to stay as the most widely used and versatile detector. Judging from the Table 1.1 drawbacks of PMTs in comparison to other types of detectors are high supply voltage and low photodetection efficiency, though large photosensitive area, commercial availability of multichannel PMTs and novel approach leading to ~100Mil max count rate presented in this thesis allow them to be a detector of choice for many fluorescence detection approaches.

Performance parameter	PMT	SPAD	SiPM
Spectral response range	200~900	200~1000 nm	300 ~1000 nm
Photosensitive diameter	large	0.1~0.5mm	0.1~3mm
Gain	10^6	10^6	10^6
Power supply	~KV	~200V	~50V
Price	~$200	~$1000	~$10
Dynamic range	~10M	~10M	10~100M
Temperature coefficient	_	0.7V/ºC	0.05V/ºC
Processing technology	Vacuum tube	Dedicated	Standard CMOS
PDE	5~20%	20~70%	20~70%
Gain varies with magnetic field	yes	no	no

Table 1.1 Comparisons: PMT, SPAD, and SiPM

1.6 Formulation of system requirements.

Our beads coloring strategy requires the ability to distinguish millions of color combinations. Problem with detecting color combination from micro-beads is that the beads are moving very fast (1-2m/s) and they emit very low amount of light.

Our solution is to develop a single photon detection with broad linearity range, fast frame rate and high data recording rate.

For a beads detection system our ultimate goal is to deliver up to 10^4 objects/s which have to be recognized with 1%-10% accuracy. In order to be able to do that we need to collect about 10000 photons per dye. Since in our spectrometer a dye spectra occupy ~ 5-6 photocathodes of PMT, our total requirements for the system goes up to having ~10^8 counts per second total. This requirement is the basis on which all the further discussed development of single photon spectrometer is based.

CHAPTER 2

DEVELOPMENT OF SINGLE CHANNEL PHOTON COUNTER

2.1 Description.

Single channel counter was the first step on the way to 32-channel high speed counter we had in mind from the start. The idea behind single channel counter was to develop the counter being able to reliably count PMT pulses from tens (right above noise floor of the PMT) up to 100 million counts per second. Upper bound was limited by ~1ns PMT pulse width and best possible switch rates of the necessary circuitry. As PMT pulses as well as photon flux incident on PMT window obeyed Poisson distribution as the number of pulses increase more and more pulses would overlap and merge with each other reducing the amount of registered photon events. Simple analysis would give us ~60% probability of having 2 or more pulses in 2ns interval at 1Ghz photon rate thus making photon counting not applicable there. At 100MHz on the other hand this probability gets reduced to only 1.7% for *initial* photon flux. This way in the ideal case when amplifying and discriminating circuits would add to noise and pulse spread to this figure, reliable counting at 100MHz would be easily possible.

According to the numbers above the faster and less noisy components we would use the closer we would be to 100 million count goal. Having that in mind we ended up with Infineon technologies 20-db BGA427 amplifiers and Analog Devices ADCMP553 LVPECL comparators for pre-amplification and discrimination circuits respectively.

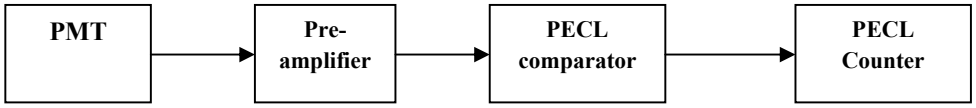

Figure 2.1 Single channel block diagram.

We can divide our processing circuit into 3 major functional blocks:

- Pre-amplifier circuit;
- Comparator;
- Pulse counter.

Over the course of development of single channel counter and, especially, the much more advanced 32-channel counter the exact types of components used in each of those blocks did changed fitting to the requirements of the device, but the very functional structure remained the same. Pre-amplifier circuit's purpose is to increase the magnitude of comparably weak PMT pulses to the triggering levels of the subsequent comparator. The exact amplification provided by this circuit has to be as low as possible to keep the pulses shape close to the original one and, at the same time, to be high enough to suit the input requirements of the subsequent comparator.

Comparator is used as a selective device to register pulses above a certain height and to cut off most of the PMT noise. This goal could be achieved by changing its threshold to the desired value.

Pulse counter has to be able to register and count all the pulses coming from the comparator and output the counted numbers into PC.

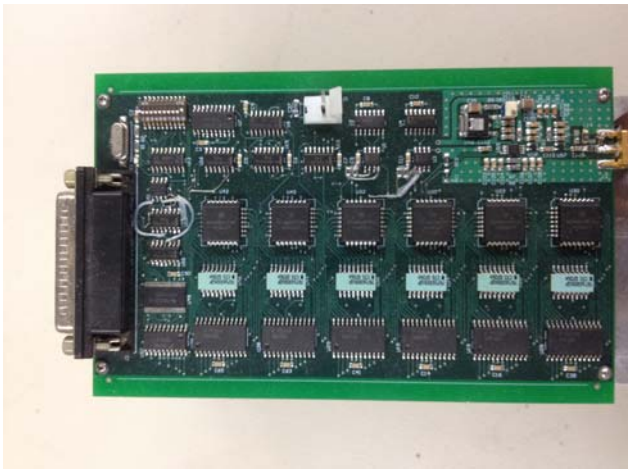

Figure 2.2 Top view on the counter board.

In the following chapters we will go into much more detailed description of each functional blocks of the single channel counter device.

2.2 Materials and methods.

2.2.1 Amplifier.

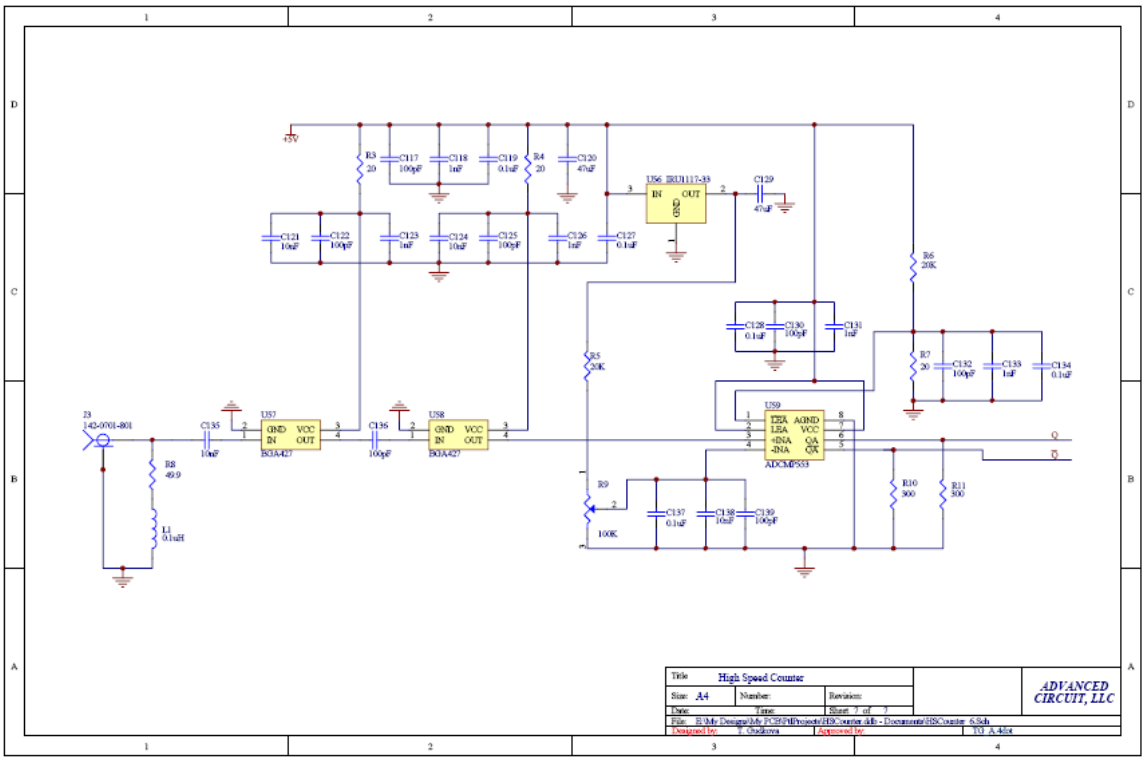

Figure 2.3 Amplification circuit scheme.

Magnitude of pulses produced by any PMT is governed by its internal gain, but even for the highest gain PMTs available on the market it lies within ~2-3x10^6 which corresponds to 10-50mV voltage pulses on 50ohm load. Pulses of that magnitude couldn't be feed directly into the digital circuits, thus they had to be pre-amplified to the necessary levels for the comparator to reliably trigger.

Since PMT produces current pulses as a result of multiple multiplication stages at the dynodes with some coefficient at each dynode and those coefficients can vary depending on

many factors, pulses corresponding to different photons can have different magnitude. This fact along with finite tolerance of comparator threshold leads to the necessity of pre-amplification of the pulses into single volts range. On the other hand if the amplification ratio is too high, the largest pulses will get into saturation region of the amplifiers or will get out of higher bound of comparator input range – in both cases that will lead to broadening of the pulses and, thus, decreasing the maximum count rates which directly contradicts our goal.

That's why we tried different amplification schemes in order to find the optimal one. We started with 2-amplifiers circuit having 2 identical BGA 427 amplifiers (U57 and U58) in cascade, resulting in ~40db total amplification (Figure 2.3). Since each of the amplifier inverted the polarity of the pulse, the amplified pulses stayed negative. The amplified signal went to the ADCMP553 LVPECL comparator (U59). The reference voltage can be adjusted using potentiometer R9 from 0 to 3.3 volts. When the negative amplified signal pulse goes to the comparator, it generates PECL-level output pulse, which goes to the counters.

The further experiments have shown that 2 stage scheme was redundant and, moreover, led to spreading of output pulses width due to the 2nd stage amplifier was reaching its saturation region too often. That was an unfavorable result for us since we strived to introduce as little distortion of the PMT pulse as possible.

Next we went through the idea of putting an adjustable attenuator to the amplifier input (which ended up as too complicated and unnecessary) and finally after a sequence of test we gave up of the 2-stage scheme in favor of single amplifier one.

Accordingly for 1-stage amplifier we got rid of U57 amplifier and C35 capacitor. The resulting scheme provided 20dB amplification and changed polarity of the pulse only once. After the amplifier the positive pulse going to the comparator, whose reference voltage needs to be set from 1.2V (middle point of the amplifier) up to the amplified pulse height. According to our tests the threshold voltage had to be chosen as close to the pulse bottom as possible at the same time having it above the noise level. Values around 1350mV were found satisfying.

Less amplification in this implementation could potentially lead to losing some very small pulses in the noise floor, but their numbers were found to be negligible.

2.2.2 Comparator.

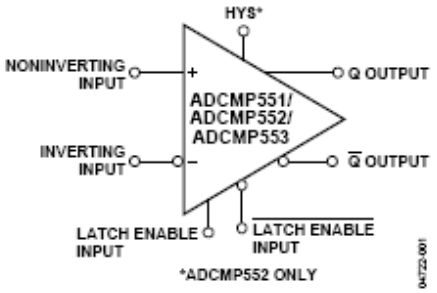

Figure 2.4 Comparator pin-out.

The choice of the comparator was one of the most important things to affect the whole performance of the device.

There have been 2 major requirements:

- highest possible switching rate;

- high noise protection.

Both requirements obviously served only one purpose - to alter the pulses characteristics as low as possible. That was the reason of choosing LVPECL logic. It provided us with exceptionally low rise and fall times (~500ps both) and very good RF noise reduction, due to differential outputs mode. Any transmission line carrying GHz signal for even a couple centimeters length encounter a lot of induced noise over the air, that's why PCB layout and choice of transmission ways had to be done very carefully.

Choice of low voltage PECL logic was quite justified by trying to overcome an intrinsic drawback of PECL-family to have high power consumption.

2.2.3 Counter.

High Speed counter contains:

- Two identical counting circuit, each containing a **Three-byte PECL counter,** 3 **PECL to TTL 3-state buffer** and 3 **AND gates**.

- Synchronization circuit, containing a fixed value unit **Sync-byte, Sync-blocks two-byte counter,** 3 **3-state buffers** and 3 **AND gates.**

- Control circuit, containing a **Crystal oscillator, 14-stage binary ripple counter, Switches, Bytes Counter, Blocks counter**, 2 **AND gates**, 1 **NOT gate**, flip-flop **FF,** and 4 **TTL to PECL converter.**

- LPT output control circuit, containing **Time Delay unit, OR gates** and flip-flop **FF.**

High Speed Amplifier pulses simultaneously get to the inputs of **3-byte PECL counter #1** and **#2.** One of these counters is always in counting mode, while the other one is on hold and its accumulated data is being transferred byte after byte to the LPT port through the **PECL to TTL 3-state buffer,** corresponding to the byte number. **Three-byte PECL counter #1** and **#2** states are determined by the *control circuit* signals converted by the corresponding **TTL to PECL converters**.

TTL to PECL converter #2 output signal sets and holds the **Three-byte PECL counter #1** into the hold mode, and the **Three-byte PECL counter #2** - into the counting mode.

TTL to PECL converter #3 output signal sets and holds the **Three-byte PECL counter #2** into the hold mode and a **Three-byte PECL counter #1** - into the counting mode.

Converter #1 and #3 output signals reset the corresponding **Three-byte PECL counter** after its data has been transferred to the LPT port.

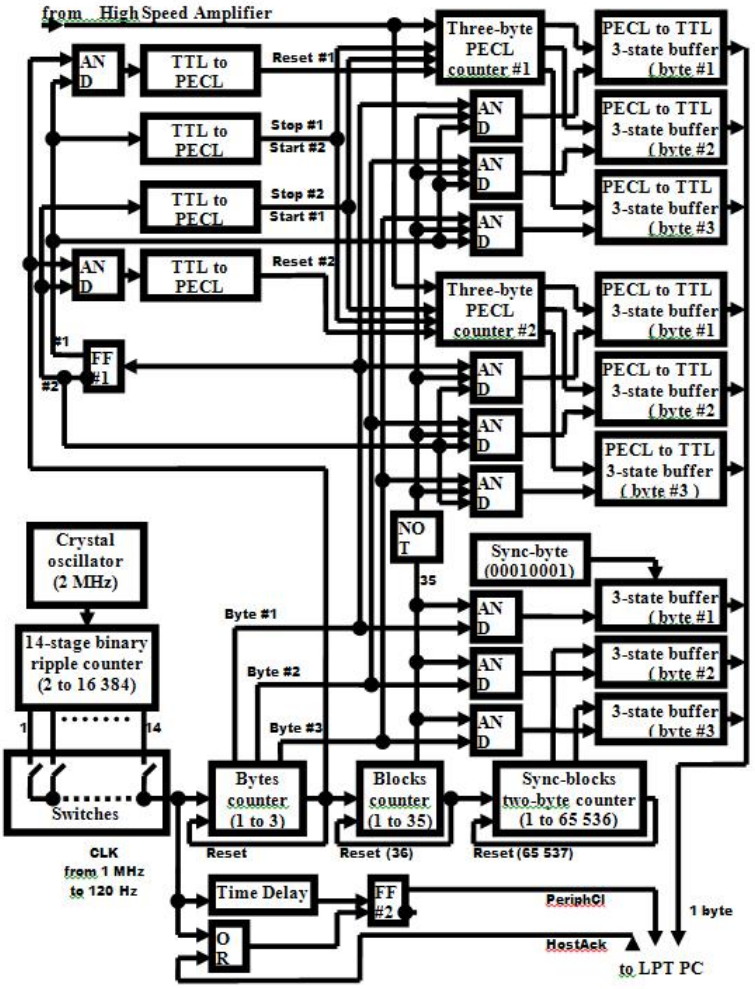

Figure 2.5 Counter block diagram.

After each 102 transmitted bytes there go the 3 synchro-bytes from the *synchronization circuit*. 1st byte has the fixed value of 00010001 and 2nd and 3rd bytes are the current state of the **Sync-blocks two-byte counter**. The synchro-bytes go the system output through the corresponding **3-state buffers.**

Crystal oscillator generates the 2 MHz clock pulses which go to the **14-stage binary ripple counter**. The counter has 14 output pins. Each pin outputs the clock pulses with the initial frequency divided by a coefficient from 2 to 16386. **Switches** are used to choose the pin

and therefore the clock frequency for the whole circuit. **Switches** can set the transmission speed of the data to the LPT port from 122 to 1 000000 bytes per second.

The clock pulses get the **Bytes Counter**. After receiving each clock pulse the **Bytes Counter** sequentially generates the signal on its 3 outputs. Each signal allows the transmission of the corresponding data byte. Each of these signals goes to the both *counting circuits* and, via the corresponding AND gate – to the *synchronization circuit*.

The high on the 4th output resets the counter. It also goes to the **Blocks counter**, which counts the number of the transmitted 3-byte words. When the transmission of the 102th data byte ends (34-th 3-byte word) **Blocks counter** generates the signal for the 35th word. This signal allows #3 **AND gates** to transmit the signals for putting the synchronization circuit's data to the LPT output. At the same time this signal (for the 35th 3-byte word) blocks the output of the *counting circuits*.

Blocks counter output signal, corresponding to the 36th 3-byte word, resets the counter and clocks the **Sync-blocks two-byte counter,** which counts the number of 105 byte sequences and resets at a value of 65536.

Flip-flop **FF#1** triggers by every 1st byte pulse of the **Bytes Counter**. Its signals alternately put **Three-byte PECL counter #1 and #2** into count or hold modes, enable/disable the output of the counters and allows/block the transmission of the reset pulse to the counters via **AND #1-4** and **AND #1-4 gates.**

2.2.4 Software.

In order to be able to store and present the accumulated data in PC we developed a software package strictly dedicated to this purpose. It consists of recording software, real-time visualization package and offline visualization package.

For single channel counter we use LPT port to transfer the data into PC. Despite being a legacy port LPT allowed us to have the integration window as low as 1ms, which provided decent time resolution for optical counts.

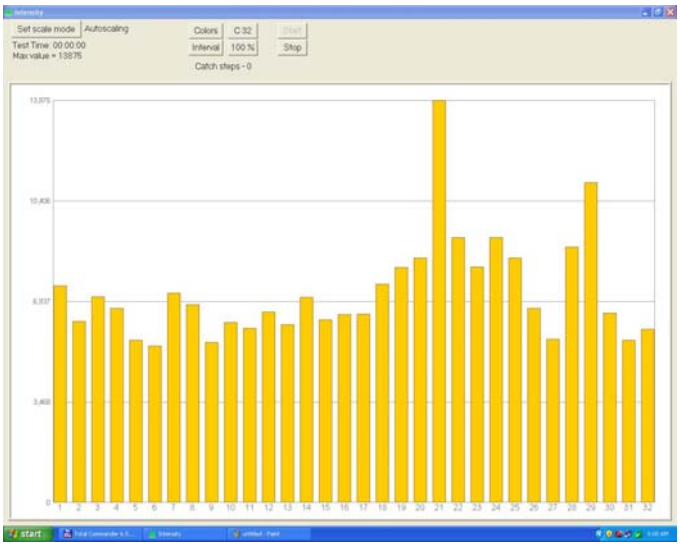

Figure 2.6 Intensity software window.

On the Figure 2.6 there's a screenshot of our 'Intensity' software. It was designed to provide a view of all the PMT channel at the same time. It is very useful to get picture of the current light conditions of the PMT and is extensively used for fine-tuning comparators' thresholds for all the channels.

Figure 2.7 Monitor software main window.

The Figure 2.7 shows us ‘Monitor’ software window which serves the purpose of recording data from LPT and forming the output data file. It is also suited to provide real-time single channel monitoring, as it can be seen on the screenshot.

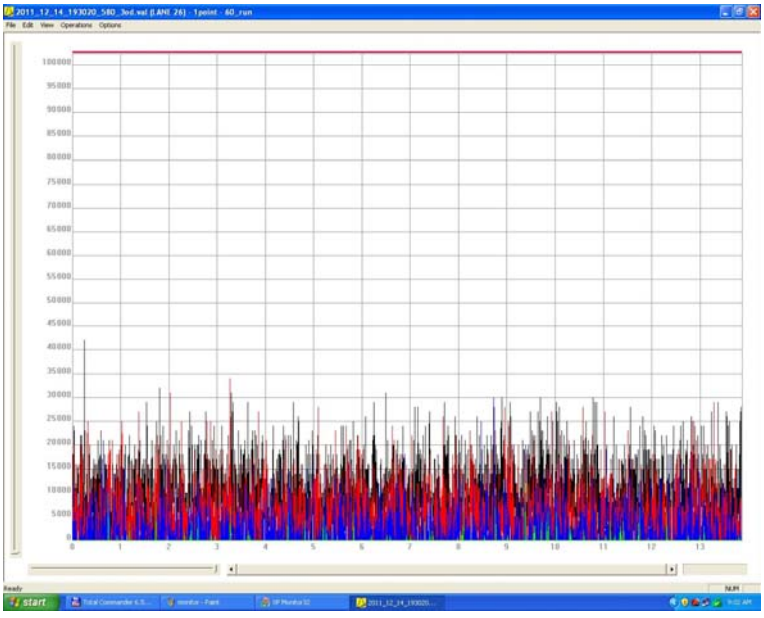

Figure 2.8 Base software main window.

And finally on Figure 2.8 we can see ‘Base’ software window which is used for offline analysis and processing of the recorded data files.

2.2.5 Optical system.

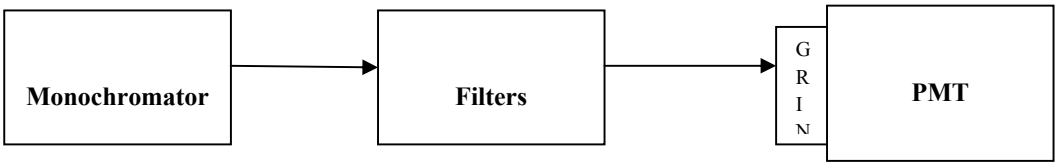

Figure 2.9 Optical system setup.

For our experiments we designed an optical system with 2 major capabilities:

- Light intensity is uniform and easily adjustable in the range from full darkness up to higher count limits of the system.
- Light spot hitting the PMT has to be as focused and confined as possible to be able to illuminate only 1 channel of the PMT.

First property was achieved by using The Optometrics Group MLM-2 monochromator which has an adjustable wavelength of the emitted light from 400nm up to 800nm. With this type of monochromator light can be easily attenuated by means of a set of neutral filters. In our case -5OD filter was almost equivalent to darkness conditions on the PMT. So using -4, -3, -2, -1 and -0.3 OD and 0 OD for no filters settings we managed to take most of our linearity curves.

Second property implementation involved a 200mkm fiber connecting SMA connector on the monochromator and a custom-made PMT header attached to the PMT front part.

Figure 2.10 PMT header before attaching to the PMT front.

The header was designed to be able to slide along the PMT front, thus directing the light on any PMT channel.

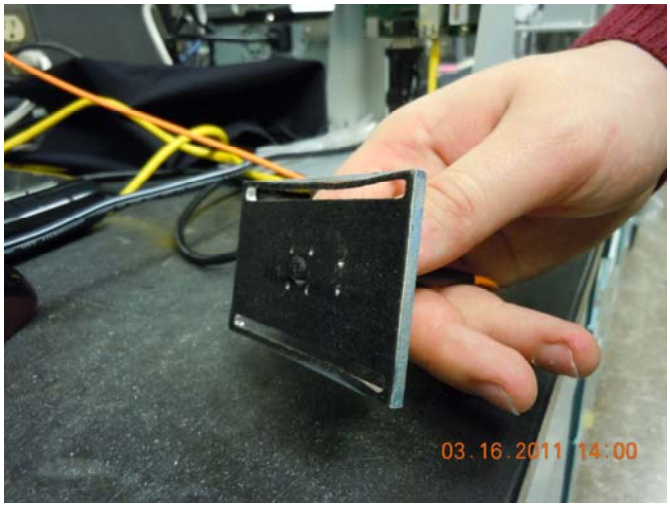

Figure 2.11 PMT header back side.

A GRIN lense was incorporated into the header to be able to focus the light onto the channel even more, thus reducing optical crosstalk by a noticeable margin.

CHAPTER 3

RESULTS DISCUSSION

3.1 PMT pulses.

Since PMT pulses width is ~1ns we had to use a high bandwidth oscilloscope to be able to capture the pulses shape. Tektronix TDS7404 4GHz oscilloscope was quite sufficient for this cause. Many of the pictures below were taken in accumulating mode of the oscilloscope which allowed us to view many pulses at once, thus displaying pulses height variations. Blue graph in the left part of the figures represents a pulses height distribution in the sample.

The following pulses have been obtained from 9th channel of the PMT for different light intensity levels. In the weak light conditions (4OD attenuation in our setup, Figure 3.1) we observed pulse height variations from ~5mV up to 70mV for single pulses. Though, according to the histogram average pulse height was at about 20mV with FWHM width of ~1ns, as it was expected for this type of PMTs.

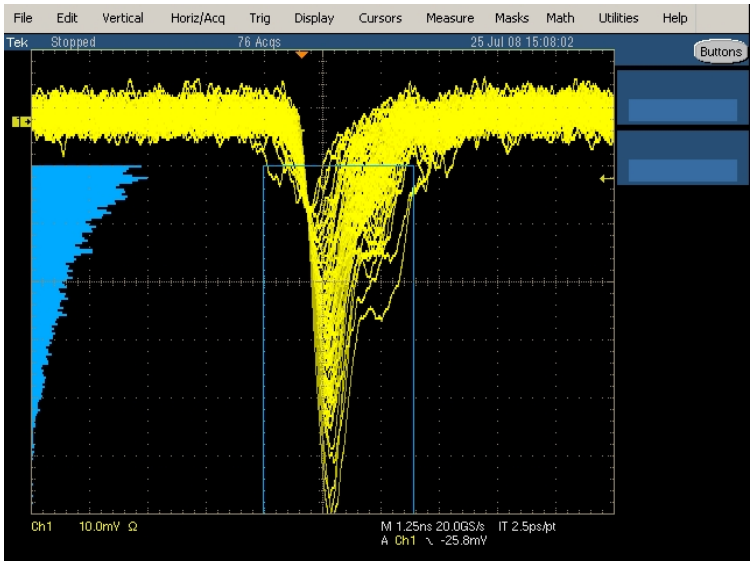

Figure 3.1 PMT pulses in weak light.

Next figure (Figure 3.2) displays pulses behavior in the oversaturation condition. Almost all the pulses are merged with the noise floor, and despite their amounts are very high our discriminator scheme is unable to register the most of them. If comparator threshold is high there're no pulses registered, if it's low real PMT pulses get mixed up with noise and counts are very high, giving us the noise picture.

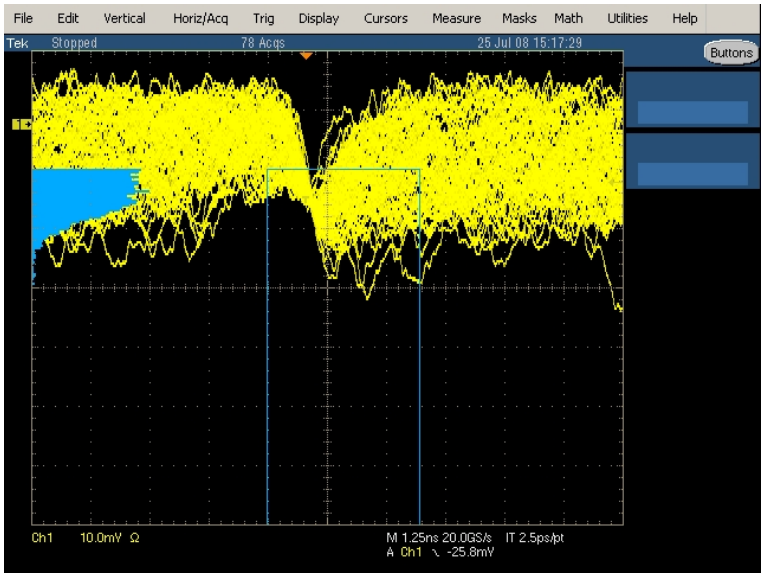

Figure 3.2 PMT pulses in very high light.

The Figure 3.3 shows changes in number of pulses and pulses heights occurring when a graduate increase in light intensity is performed. In can be easily seen that pulses stay 'valid' up to 1OD measurements (7^{th} screenshot from top left on Figure 2.3), then an interesting behavior is observed. As the light increases further not only the number of pulses goes up, but their amplitude goes down as well. We explain it by PMT going out of its working conditions, thus producing many additional pulses per each real one. Though number of counts registered by the counter goes down, as most part of the pulses appears below its threshold (set up for working

condition) and its ability to tell one pulse of another also gets reduced, since the pulses overlap each other.

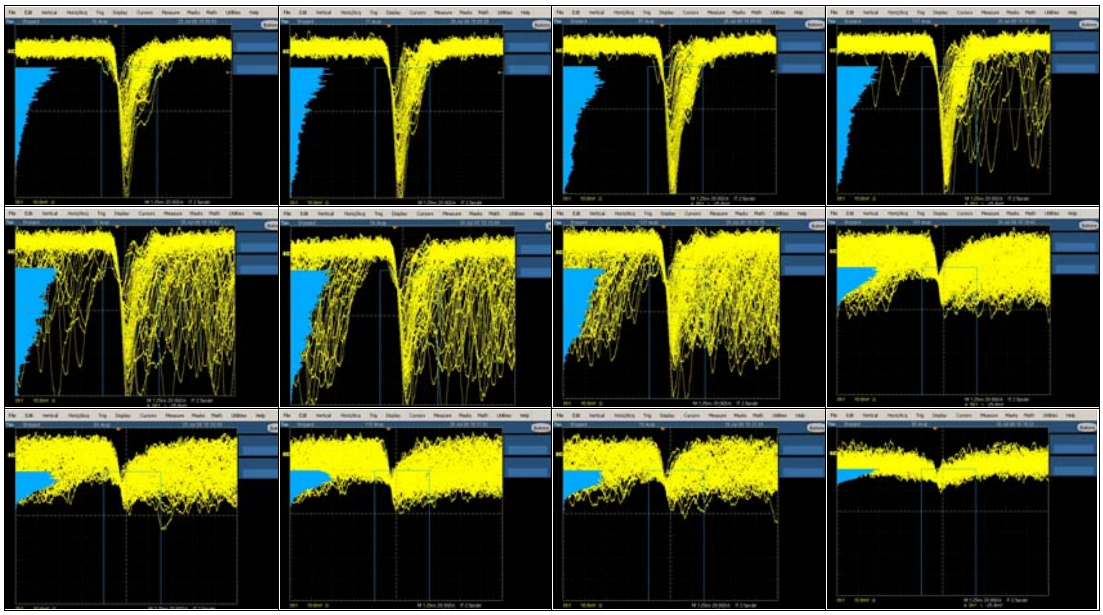

Figure 3.3 PMT pulses in the range from darkness to very high light.

Judging by the pulses shapes it's reasonable to conclude that up to 1OD PMT has to be close to the linear mode. At 1OD the pulses are still close to the valid ones, by there has to be some deviations from linear characteristics and at higher light PMT behavior has to be highly non-linear. And it appears to be just the case in our linearity discussions in a chapter below.

3.2 PMT vs. Comparator pulses.

Since the performance of the whole system heavily relies on comparator switching capabilities it's important to compare pulses going out of the comparator to the initial PMT

pulses. This way we can tell how wider the pulses become after the comparator and thus what are the pulses our counters have to deal with.

We had 1-stage amplifier scheme and 2-stage amplifier scheme to test and compare.

3.2.1 One-stage amplifier.

On Figure 3.4 we can see pulses taken at the comparator output (cyan) versus pulses on the comparator input (yellow) for different light intensities and thus number of pulses. It appears that comparator pulses are at ~2ns width, compared with amplifier pulses of 1ns. This pulses widening was expected from comparator characteristics and is very good for pulses counting purposes. For any pulse height comparator response is unchanged.

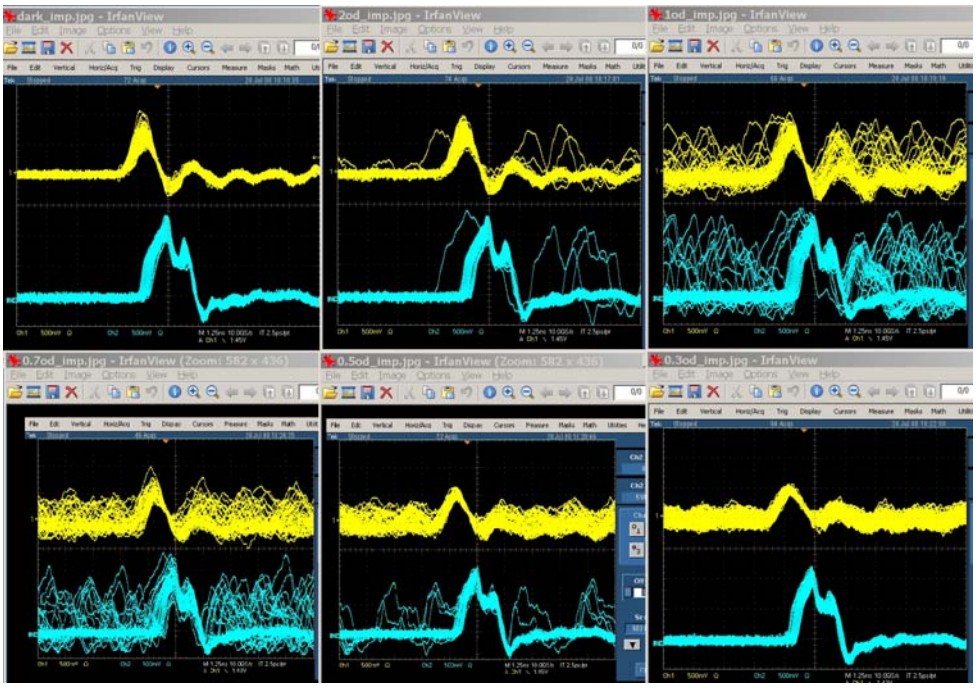

Figure 3.4 One-stage amplifier vs. comparator pulses.

3.2.2 Two-stage amplifier.

For our 2-stage amplifier, using the same optical part, we obtained the following pictures, clearly showing the spread of the pulses after comparator or, which is equivalent to the pulses width after 2^{nd} amplifier added to <1ns increase by the very comparator.

At Figure 3.5 top 2 graphs PMT pulses are small and comparator output is close to 1-stage amplifier case above, but bottom 2 graphs of Figure 3.5 shows what happens if the pulses are large. Comparator pulses became much wider (about 5ns) than expected and reasonable to use.

We investigated this rather unexpected spread and found out that the cause of it is the fact the amplification is too large. The pulses after first amplifier put the second amplifier's transistors into saturation region causing the spread. This performance was found unacceptable and we gave up with 2-stage amplifier scheme altogether.

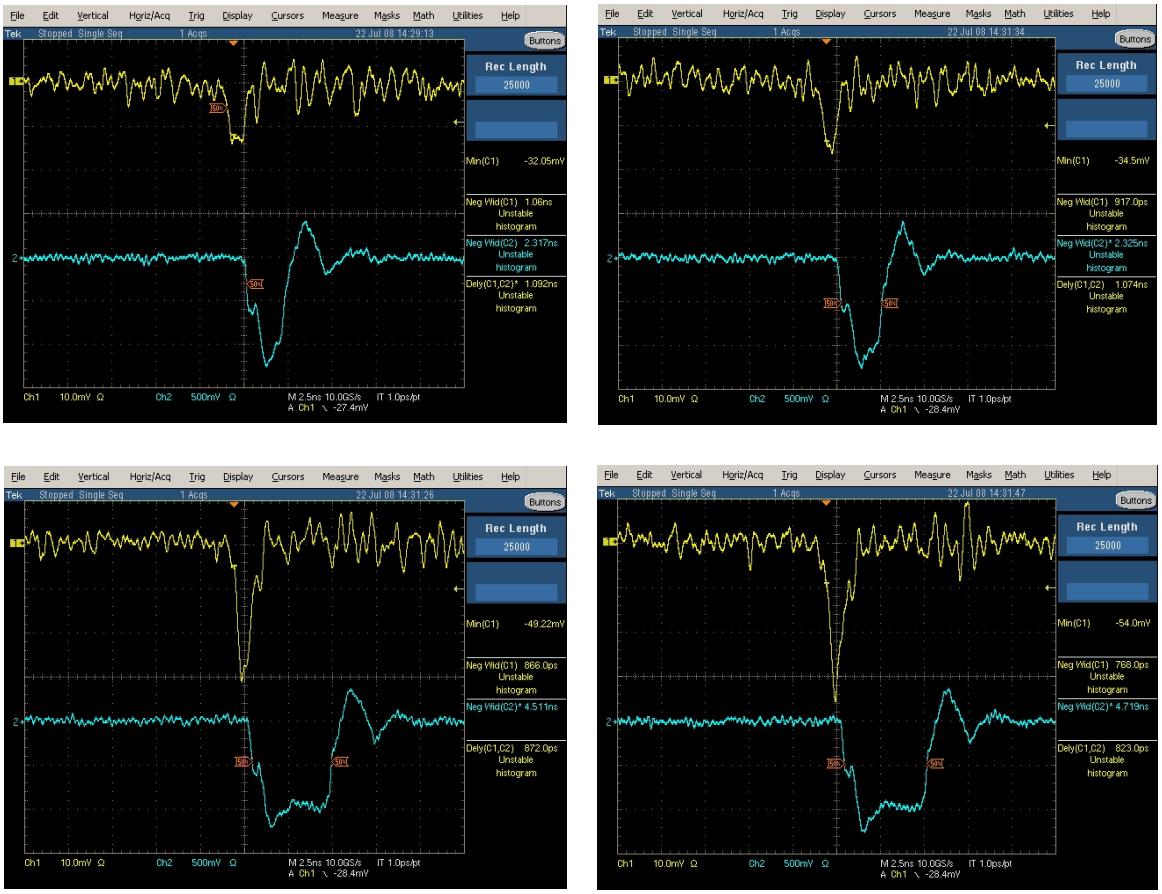

Figure 3.5 Two-stage amplifier PMT vs. comparator pulses.

3.3 PMT counts linearity.

Our goal of achieving 100 million counts per second is two-fold. First we need to demonstrate the very ability to get to 10^8counts and second, which is equally important, to show that that high counts lie within linear range of the device. That's why linearity measurements are the key performance characteristics of the counter.

We assembled the setup on figure 3.6 for linearity measurements.

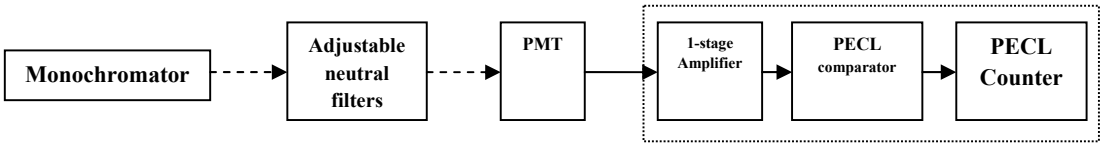

Figure 3.6 Linearity measurements setup.

Then we fixed the wavelength in the area of high PMT response and went through our set of filters at -4, -3, -2, -1, -0.3 and 0 ODs to capture the counts from the device.

The data has been taken for different comparator thresholds in attempts to find out how exactly different thresholds affect linearity characteristics.

Since our counter was designed to operate in 2 modes: 1-byte data per time interval and 3-bytes data per time interval, we needed to compare those modes too.

Figure 3.7 shows linearity curves for 4 separate cases. The graph is in log scale and we can expect that perfectly linear curve will be close to red dotted one. This way we can easily see all the deviations from linearity for different experiments.

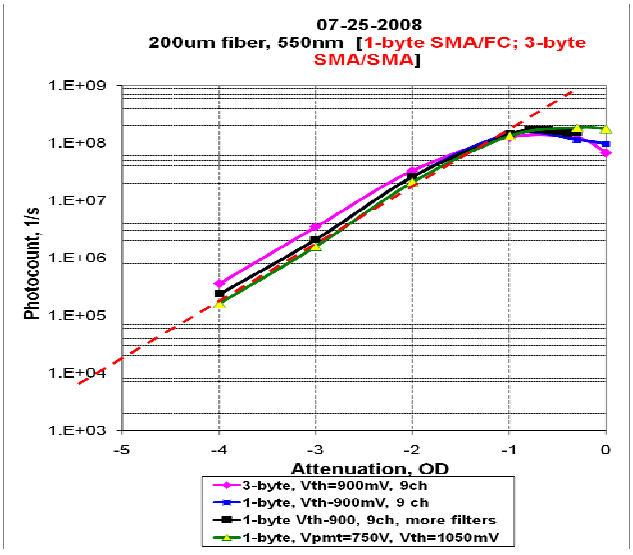

Figure 3.7 Linearity curves for 4 different counting schemes.

As it can be seen from the figure all curves are very close to each other and their behavior can be described using 3 distinct ranges of light intensity:

- From -4OD to -2OD – perfect linearity of the device. 20-30 million counts.
- From -2OD to -1OD – slight deviations from linearity, because some pulses start to appear below comparator threshold.. These deviations they can be easily corrected by post-processing. 'sub-linear' region. Up to 100 million counts.
- From -1OD to 0OD – Non-linear range.

The next figure (Figure 3.8) shows linearity curves for different threshold voltages. The results one more time confirm that the closer the threshold voltage is to the bottom of the pulse – the more pulses are registered – better linearity curve, until the point we start registering the noise floor. The closer we are to the noise floor while not touching it – the more linear characteristics are. Though it can be easily seen the graphs starts going down earlier, if we're very close to the noise floor, thus putting a limit on the highest count rate.

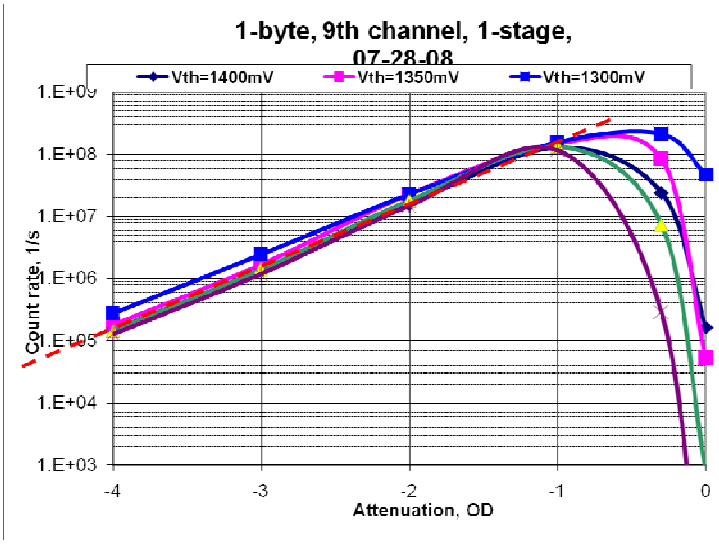

Figure 3.8 Linearity curves for different comparator thresholds.

It emperically follows from the Figure 3.8 that the threshold of 1350V is the best tradeoff between perfect linearity and highest count rate. That's why we've chosen this threshold for the following experiments.

Now our goal was to compare linearity curves for the same threshold by for different wavelengh of the incident light.

The Figure 3.9 shows 3 characteristics of 1-stage amplifier PMT counts for 3 different wavelength. For all 3 of them the output remains linear until more than 10^8 counts. Difference in absolute counts numbers for 488nm&530nm case VS 630nm is easily explained by PMT quantum efficiency characteristics, which have a peak around 450-500nm and a decreasing slope for 600+nm wavelengths.

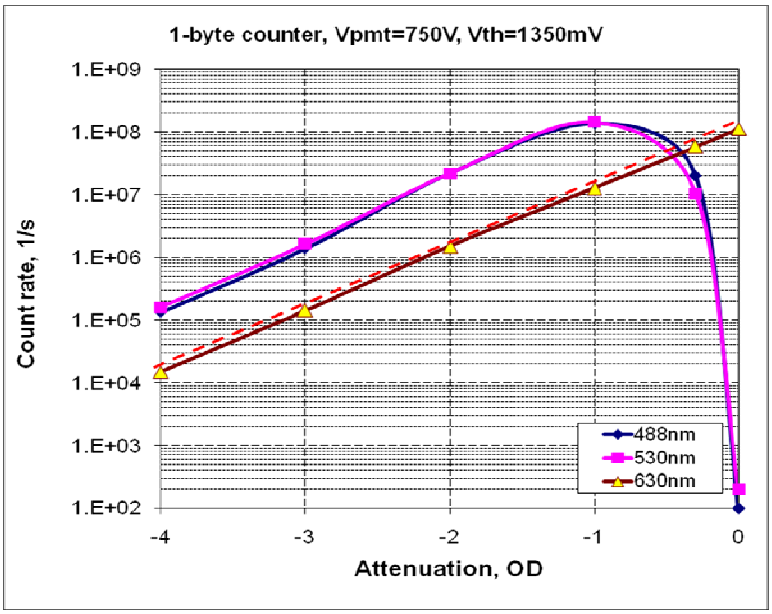

Figure 3.9 Linearity at different ligh wavelengh.

3.4 Crosstalk.

Next important investigation we had to perform is to measure how much the channels of our multichannel system affect each other. This is called channels crosstalk of a multichannel system. The crosstalk is an inevitable property of any kind of multichannel system when the channels are not totally separated from each other. In our case the common spots where crosstalk may occur are optical bench and its capability to focus and direct the beam of light in one single channel only and internal electronic crosstalk inside PMT or on the board itself.

Measuring channels crosstalk in multichannel PMT is very important to make corrections into all further signal measurements.

The crosstalk as it was mentioned earlier can have 2 different origins:

- Optical crosstalk, arises from illumination of a neighboring channel due to non-perfect aligning of light emitting fiber or parasitic light reflection inside the optical bench;
- Electronic crosstalk, arises from internal link between channels in PMT (amplification path is the same for all channels).

We have to note here that 'some' amounts of both types of crosstalk are the property of the device composition and cannot be reduced beyond some point.

To minimize optical crosstalk in our investigation we used a 532nm Ar-ion laser as the light emitter instead of the monochromator. Resulting light spot in the case of the laser will be much more confined and thus will provide much less exposure of the neighboring channels.

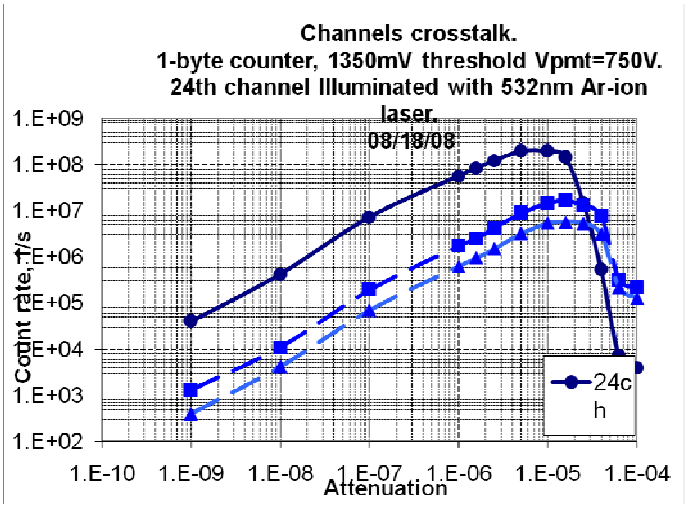

Figure 3.10 PMT channels crosstalk measurements.

What we expected to obtain is if our crosstalk is mostly optical then neighboring channels will continue to rise while the illuminated channel will get saturated and abruptly gows down. And it's mostly electronical if the neighboring channels will follow the main channel even before they would get saturated themselves.

In the results on Figure 3.10 neighboring channels (2 lower light blue plots) are indeed following main channel pattern long before they got to 100mil cou nts. And their relative magnitude stay within 5% of the main channel which is what we expected from this type of PMT, having ~3-5% internal cross talk.

3.5 Poisson characteristics and comparator threshold.

Since the noise in photon counting system is determined by incident photons fluctuations noise we can expect that the if our system doesn't serve as a significant source of noise the registered counts distribution will follow Poisson distribution as well.

During the course of our experiments we observed abrupt decrease of PMT pulses height and consequitive decrease in number of registered counts at high light intesities.

To find out the nature of this phenomenon we decided to proccess the counts we obtain whether they still follow the Poisson distribution for the light intensities higher the point we get the counts going down.

We used the same setup as for linearity measurements, but this time we accumulated a large number of count-per-time interval values and proccessed them. 3 different comparator thresholds (1300mV, 1350mV and 1500) have been chosen to find out which one gives us more adequate results. Lower comparator thresholds allow us to register more pulses and making our counts distribution closer to the Poisson one (presumebly the PMT pulses follow Poisson distribution), but if the threshold is too low, we would start registering noise floor. This would effectively shift our counts distribution further from Poisson.

Higher threshold as though helps us get rid of registering noise, more and more PMT pulses become lower the threshold as we pull it up and the counts will be lower.

The following set of histograms takes all counts in a large interval, then divides them into equally distances bins and plots number of events in a bin versus bins positions. This way we can expect the shape of the plots to be close to normal distribution (good approximation for Poisson when number of events is high enough) if the events follow Poisson distribution. And vice versa the shape will get more and more corrupted if the events stop follow Poisson because of pulses overlapping, threshold getting too close to the noise floor or pulses magnitude getting below fixed comparator threshold for very high light intensities as it was observed in pulses shape discussion earlier.

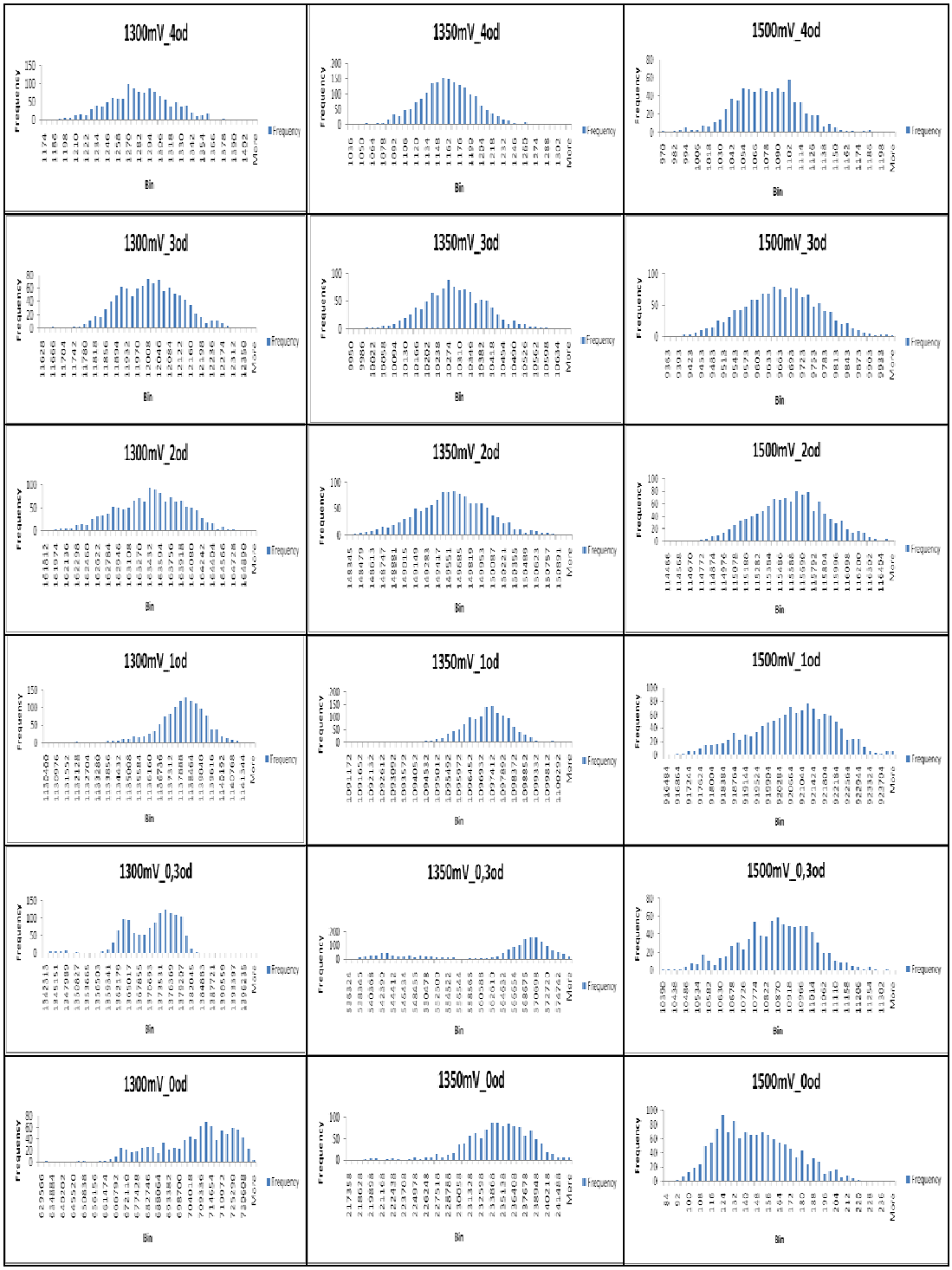

Figure 3.11 Distribution of counts at different light intensities and comparator thresholds.

As it was expected from linearity measurements the counts distribution remains close to Poisson up to 1OD attenuation But starting at 0.3OD level for 1300mV and 1350mV (which are ‘lower’ thresholds, comparing to 1500mV) the distortion gets into play and corrupts the shape of the distribution.

For 1500mV the distribution behaves slightly better, but it should have been expected as this threshold is much higher. Though even at this threshold 0.3OD and 0OD looks very different which once again tells us those light intensities are out of range of the devices performance.

CHAPTER 4

DEVELOPMENT AND APPLICATIONS OF 32-CHANNEL SPECTROMETER

4.1 Description.

In the result of the discussion we had in the previous chapter we described a working prototype of one channel photon counter. Since it proved to be a realization of our goal of having both high sensitivity and high time resolution we went on to the development of 32-channel counter device.

Since one of its major applications is supposed to be fluorescence spectrometry special type of optical head has been developed to decompose the incoming light into line spectra, as it can be seen in the figure 4.1.

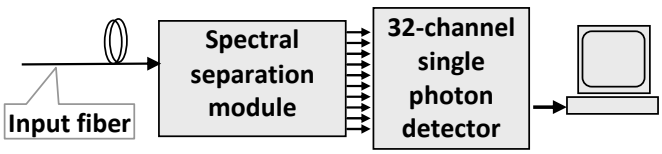

Figure 4.1 32-channel spectrometer setup.

The detector module the same as in 1-channel counter case consists of pre-amplifier circuit, discriminator circuit and counter circuit. Amplification scheme has left to be the same as

in 1-channel counter case, since the amount of amplification was found to be optimal for the subsequent comparators.

This time, as a counting circuit we used one of the fastest FPGAs available at that time, namely Xilinx Virtex-5 series one. It can provide a high level of versatility onboard being able not only to count the pulses and create the output sequence into the PC, but also potentially implement some levels of DSP directly onboard. One of the key criteria in favor of the particular type of the FPGA was its high bandwidth, which is around 1.6GHz in the case of Virtex-5. Considering the fast that ~1ns pulses from PMT are getting some spread nevertheless originating from both amplifier and comparator, the pulses on the FGPA inputs have a typical width at about 2-3ns, making 1.6GHz a suitable bandwidth to be able to register the pulses of that width. Since the FPGA didn't have lvpecl inputs we swapped the comparator used in 1-channel counter to a LVDS one, with similar speed specifications.

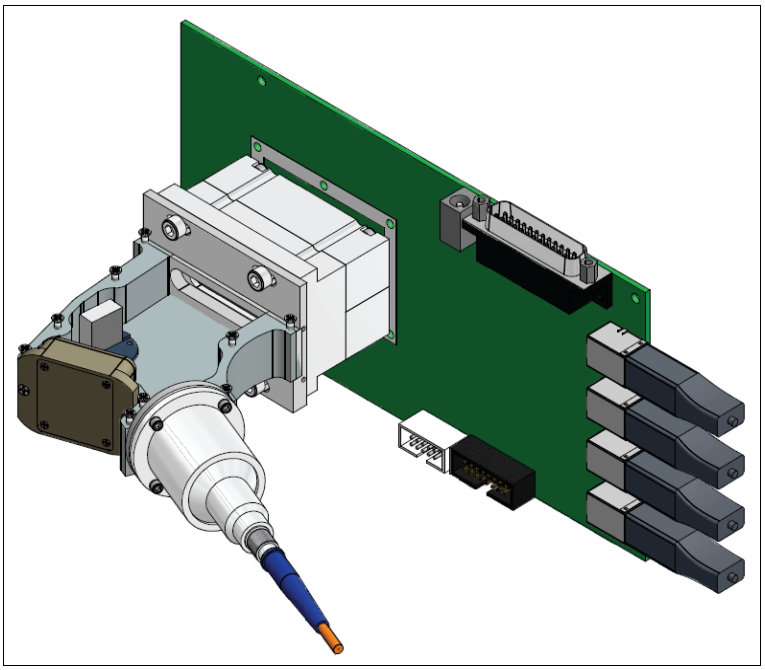

Figure 4.2 3D model of the assembled spectrometer board with attached PMT.

General looks of the device can be seen on the Figure 4.2. Unlike the 1-channel counter, the 32-channel counter has 4 USB ports as a primary means of communication with PC, thus considerably increasing the maximum data rate, comparing to LPT. Indeed, we've been able to achieve up to 1MHz counting speed per channel, totaling to up to 32MB/s overall output data rate from the whole device. Which is a large improvement over 1KHz maximum count rate of 1-channel counter. This way integration time can be brought to as low as 1usec, thus giving a very high time resolution which can be very important for many life sciences imaging applications or quantum beads detection. Data output using our custom-made software have been proven to be stable and error-free at the maximum speed over ~10 hours continuous recording.

Top view on the 32-channels counter board is provided on Figure 4.3. PMT is mounted on the center part of the board. The amplification circuits and comparators had to be situated as close to the PMT outputs as possible to prevent unnecessary signals distortion. All analogue parts are physically separated from digital ones, to reduce influences. FPGA governs all digital processing and a separate Cypress CY7C68013A usb-controller performs all communication with PC over USB output.

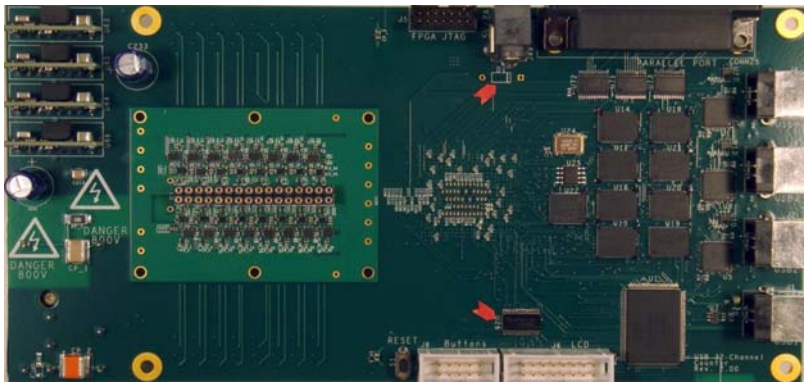

Figure 4.3 Top view on 32-channel spectrometer PCB.

LPT output is also supported and can be used when measuring slower changing signals. General looks of the assembled device in its box can be seen at Figure 4.4.

Figure 4.4 Top view on the spectrometer in the box.

It's a top view, with the board with attached PMT in the center-left part. Lower-right part has the 5V power supply for the whole device and the fiber connecting spectrometer with the SMA jack on the outer side of the box.

Frontal panel on the Figure 4.5 has a display and control buttons which allows us to choose data modes the device is capable to work. Possible modes include a choice of each of its 4 USB outputs, LPT output mode and different framerate settings for every output.

Figure 4.5 Frontal panel of the 32-spectrometer.

4.2 Spectral separation module (optical head).

Since compared to the single channel counter now the light has to be guided into a linear array of 32 channels we developed a special optical head specifically designed to accommodate spectrometric experiments.

As it can be seen on Figure 4.6 the optical head consists of fiber input with a filters holder space and the optical bench. The whole construction firmly attached to the front of PMT case.

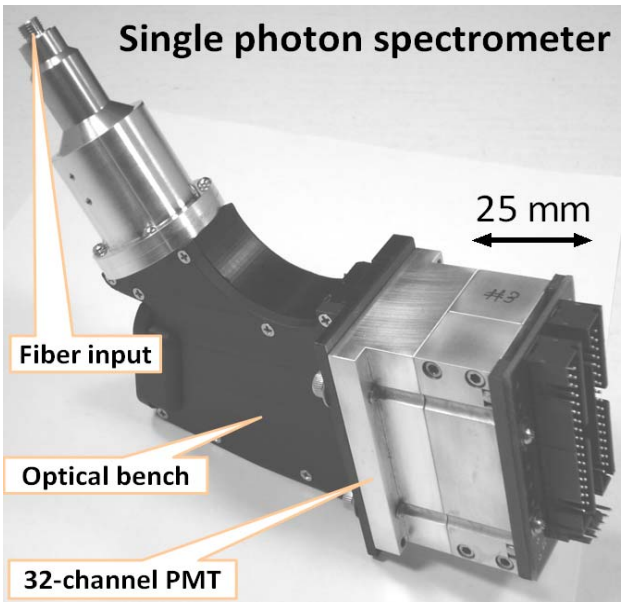

Figure 4.6 Photo of optical head for 32-channel spectrometer.

The spectral separation module performs the separation and the measurement of light in the range of wavelengths from 480nm to 670nm. The light is brought into the spectrometer through the input fiber coupled to the collimator (F810SMA-543, Thorlabs Inc, NJ, USA) which produces a parallel polychromatic beam of ~10mm diameter.

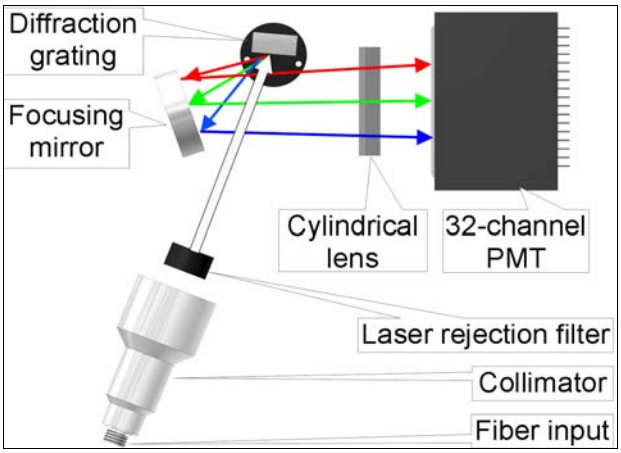

Figure 4.7 Light propagation through the optical head.

The parallel beam passes through laser rejection filters and undergoes separation on the diffraction grating (GR13-1850, Thorlabs Inc, NJ, USA) into constituent wavelength components (Figure 4.7). The separated monochromatic beams are focused onto channels of the 32-channel PMT (H7260-20, Hamamatsu, Japan) by the system comprising spherical mirror (CM254-075-G01, Thorlabs Inc, NJ, USA) and cylindrical lens (LJ1095L2, Thorlabs Inc, NJ, USA).

4.3 Pulse shapes.

Since we're using a different comparator with different output signaling (lvds vs lvpecl) we can expect to have a different pulse shapes on its output. The Figure 4.8 represents pulses after PMT on the left and pulses after the comparator on the right.

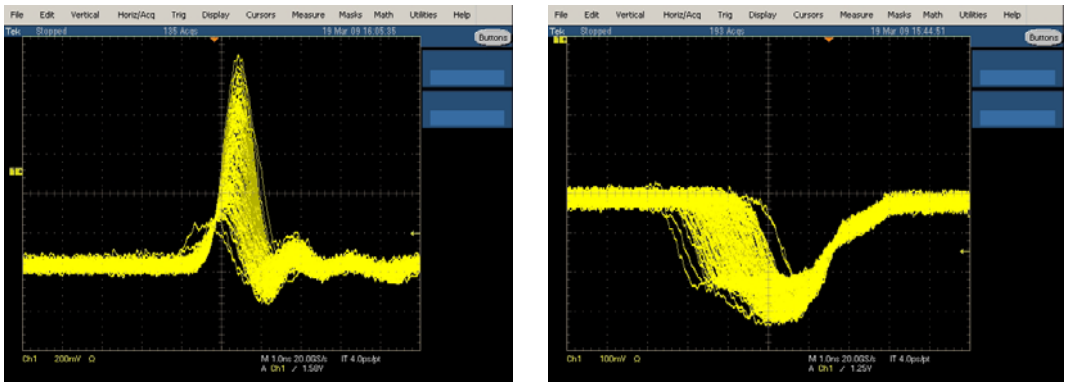

Figure 4.8 Pulses after PMT (left) and comparator (right) in 32-channel spectrometer.

We have to note, that comparator pulses though being <4ns with average about 2.5ns are good suited for photon counting purposes LVPECL comparator had slightly better timing

characteristics. Though a slight hit onto linearity characteristics comparing to single channel case could be expected and was indeed observed in the discussion in the following chapter.

4.4 32-channel spectrometer linearity.

As well as in the case of single channel counter we performed extensive measurements of the linearity of all 32 channels of the device. Test setup (on Figure 4.9) was very similar to the single channel case.

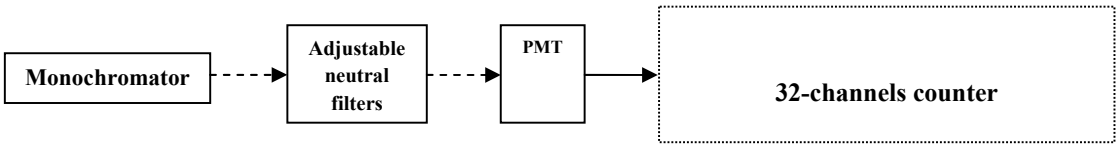

Figure 4.9 Multichannel linearity measurements setup.

We used the same single channel PMT header and focused it on each channel in turns. One arbitrary chosen channel result is shown on Figure 4.10 and multichannel results on Figure 4.11.

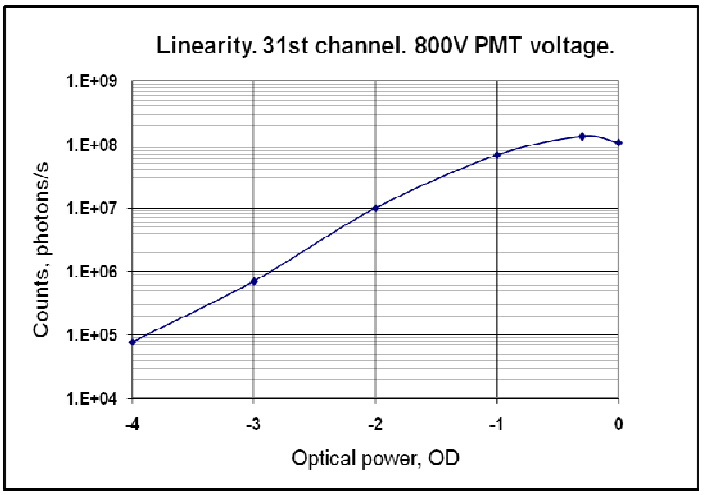

4.10 Single channel linearity curve.

As we can see on the graph, the linearity of the 32-channer counter is slightly worse than in case of single channel counter mostly due to different comporators used.

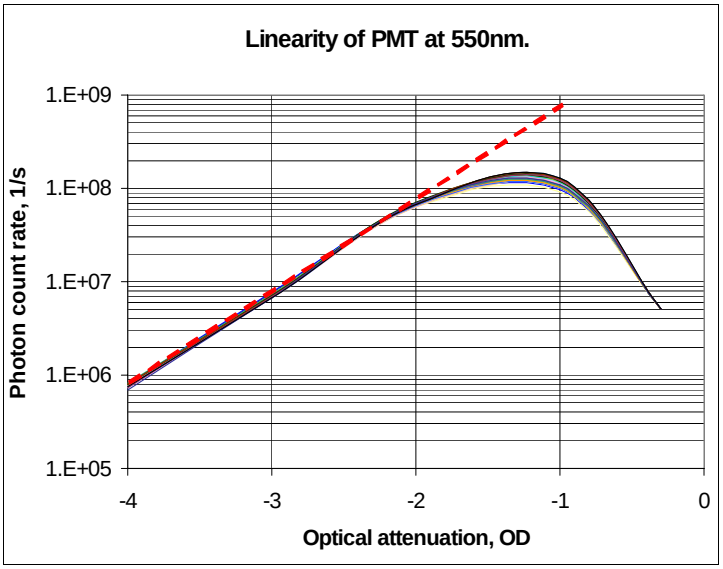

Figure 4.11 Multichannel combined linearity curves.

Another reason for the notable difference in linearity curves arose due to the fact we had to move comparators's thresholds oven further from the noise floor as different abmient conditions may and have resulted in slight variation in setup performance resulting in thresholds occasional touching the noise floor if there are too close to each other. Nevertheless despite the fact that we made considerable changes into the components of the device the performance ended up to be only slightly worse than in our prototype single channel case and almost perfect linearity was achieved up to 60-70 millions counts per second. With correctabale by post-processing linearity reaching 100-110 millions counts per second.

4.5 Spectral characteristics.

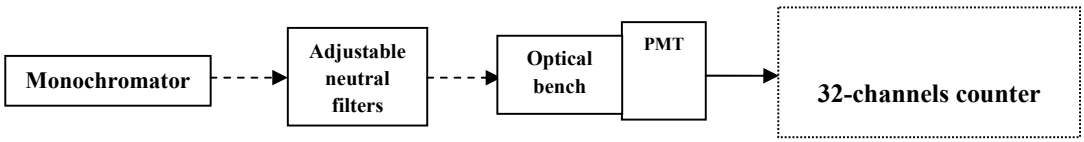

Figure 4.12 Spectral characteristics measurements setup.

In order to take spectral characteristics of the whole 32-channel device we used a modified setup (Figure 4.12) comparing to linearity measurements. Monochromator is used to gradually alter the incoming light's wavelength from 520nm to 740nm. This way each channel will have a different wavelength on it and if we will do continuous recording from all the channels we will be able to plot spectral response of the whole device.

In order to characterize the spectral separation module we connected the input fiber of the spectrometer to a monochromator. We found that the wavelength resolution of the sensor is ~10nm per channel. Analysis of the spectral separation module of the spectrometer shows that it can provide spectral resolution as high as 1nm. The obtained spectral resolution of ~10nm is determined by the geometry of the 32-channel PMT which comprises 0.8mm×7mm detection zones separated by 0.2mm distance. The overall resolution of the sensor can be improved by using an array of photo receiving fibers connected to single photon sensors.

Below (Figure 4.13) are the typical spectral response plots from the 32-channels counter in linear region:

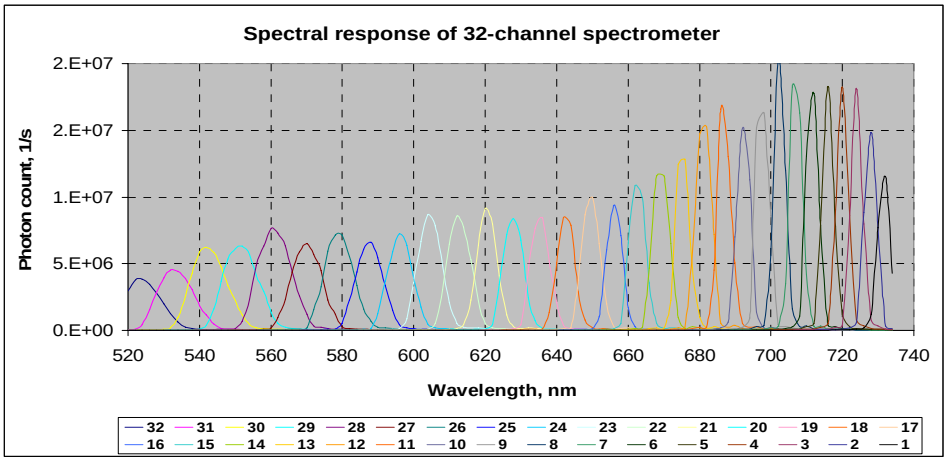

Figure 4.13 32-channels spectrometer spectral response in 520-740nm range.

As seen on Figure 4.13 each channel has a wavelength with uniquely corresponds to this channel with this setup of the spectrometer. That's why we can do a reverse plot of intensity vs. channel number instead of wavelength and get a similar type of plot (Figure 4.14)

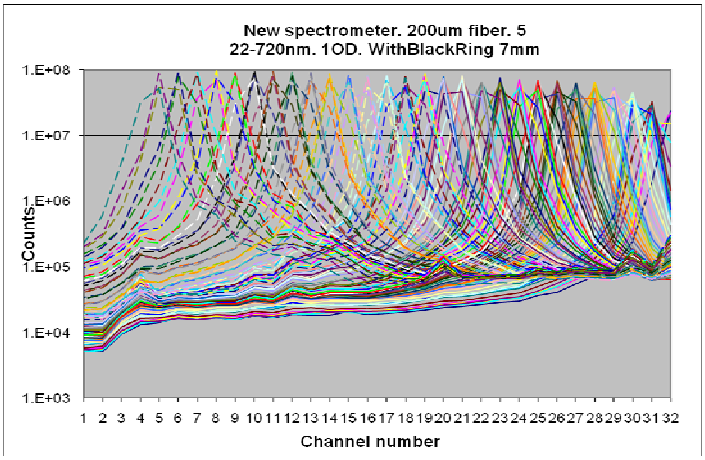

Figure 4.14 Counts vs. channel number spectral response plot.

We're able to 'shift' the whole wavelength picture by either rotation the diffraction grating inside the optical bench or by shifting optical bench along the front of the PMT case. Both ways combined we can cover the range from ~450nm up to 800nm with this device.

4.6 Dark counts and noise.

The noise in the photon counting system is determined by the temporal distribution of photo-counts. In a correctly operating photon counter we observe Poisson distribution of the photocounts for which the variance of the photo-count rate estimate is equal to its mean value, setting the lower boundary for the signal-to-noise ratio of the photon detector. In order to determine the distribution of photocounts in our detector, we collected photocounts during 25ms intervals for different light levels and recorded using our data recording software for ~30 min (Figure 4.15). The obtained good match between mean values and variances for all illumination levels indicate that the measured noise is only caused by the stochastic nature of the photon fluxes detected by the detector and that the detector itself does not produce any additional noise.

As it's expected the results are quite similar to single channel counter noise discussion in previous chapters.

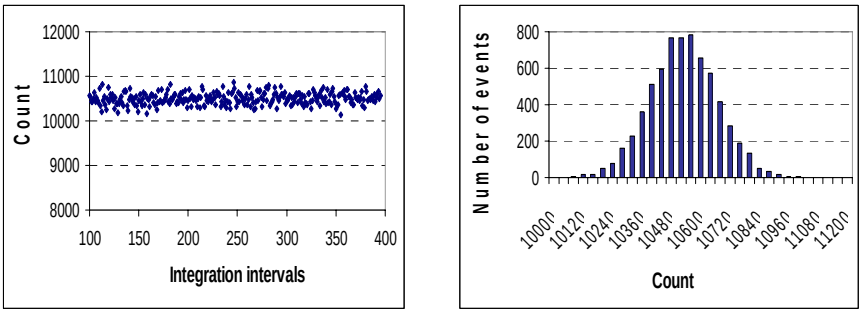

Figure 4.15 Counts distribution in 32-channel spectrometer output.

As we're using a different comparator in 32-channel counter opposed to single channel counter case we performed additional investigations of valid threshold level and obtained the plot on Figure 4.16.

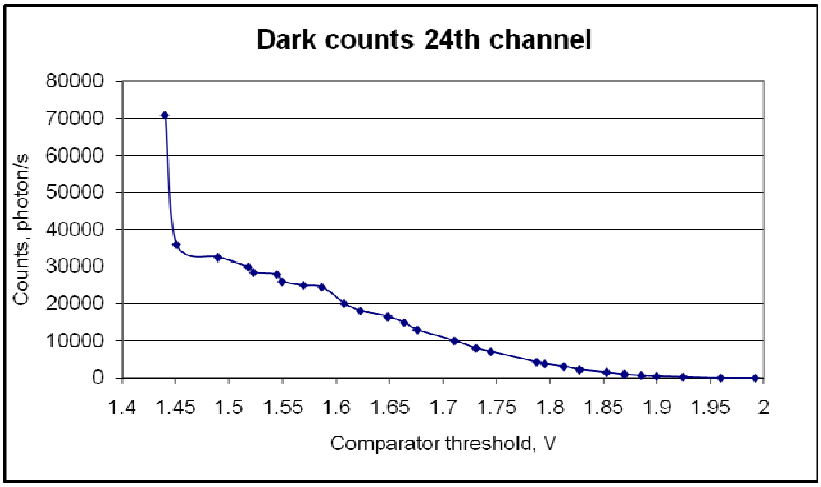

Figure 4.16 Dark counts relation on comparator thresholds.

It can be seen that any threshold value between 1.45 and 1.55V is suitable for comparators' threshold though due to channels non-uniformity exact figures has to be determined individually for each channel.

4.7 Measurements of quantum dots mixtures using 32-channel spectrometer.

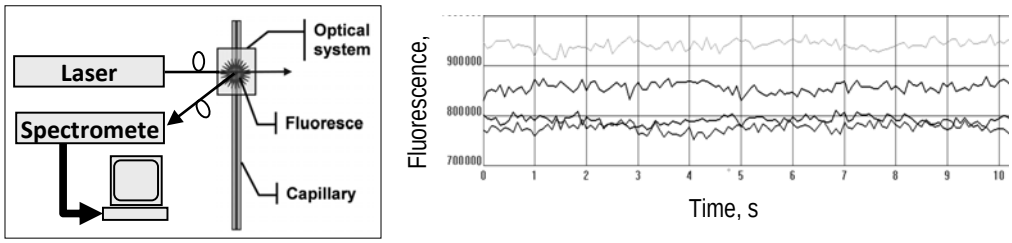

Figure 4.17 Schematic of the measurement setup (left) and typical fluorescent signal from solution of QDs in toluene recorded in four channels of the spectrometer during 10 seconds (right).

Block diagram of the setup for measurements of fluorescence spectra is shown in Figure 4.17. In the setup, a substance to be analyzed is placed in a capillary which is inserted into a fiberized optical system (see [9] for detailed description of the optical system). Fluorescence in the analyte is excited by Ar-ion laser (488 and 514nm, Uniphase, CA, USA), collected by the fiber (200mkm core diameter) and delivered to the spectral separation module. Detection of the capillary content may be done by either pulling the capillary through the optical head using a programmable stepper motor or pumping the analyte through the capillary using a programmable micro-pump.

In order to test the proposed method for detection and recognition of mixtures of quantum dots as well as the developed software for simulation of the single photon spectrometer, we have carried out measurements of mixtures of three different types of QDs with strong spectral overlap (Figure 4.17). QDs re-suspended in toluene 1mg/ml were obtained from Crystalplex Inc, Pittsburgh, PA.

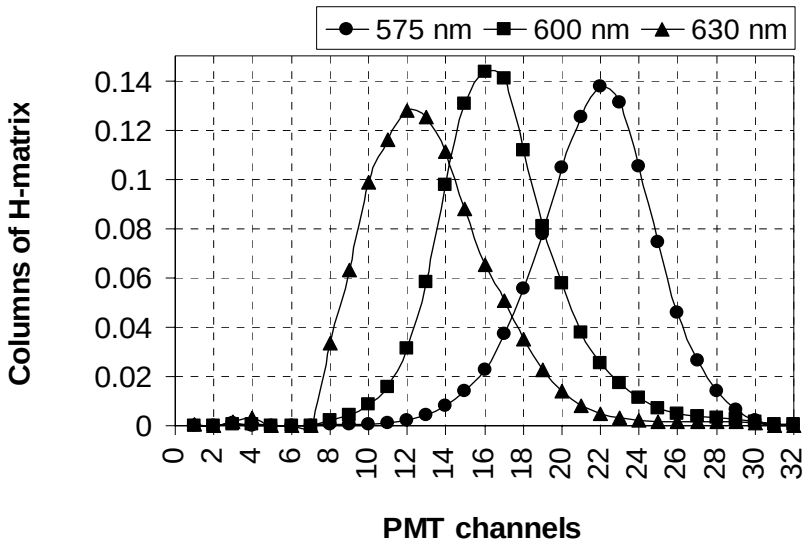

Figure 4.18 Spectra of individual quantum dots.

We premixed 50% of 575 nm QDs and 50% of 630nm QDs and prepared a series of mixtures in which the content of 600nm QDs varied from 0% to 15%. Mixtures of quantum dots were placed into fused silica capillaries with transparent coating (360um OD, 100um ID, Polymicro, AZ, USA. The total recording time for each mixture was about 5 minutes with minimum integration time of ~20ms which provided approximately 15,000 data points per mixture. The color deconvolution procedure described in Section 2 was applied to photocounts obtained in 32 channels at each data point during 20ms photon integration time. In order to increase the photon integration time, we added photocounts obtained from several sequential data points and thus applied the color deconvolution procedure to longer time intervals.

Based on the measured spectra of individual QDs we have determined the **H**-matrix and carried out color deconvolution procedure. The obtained results are presented in Figures 4.18 and 4.19.

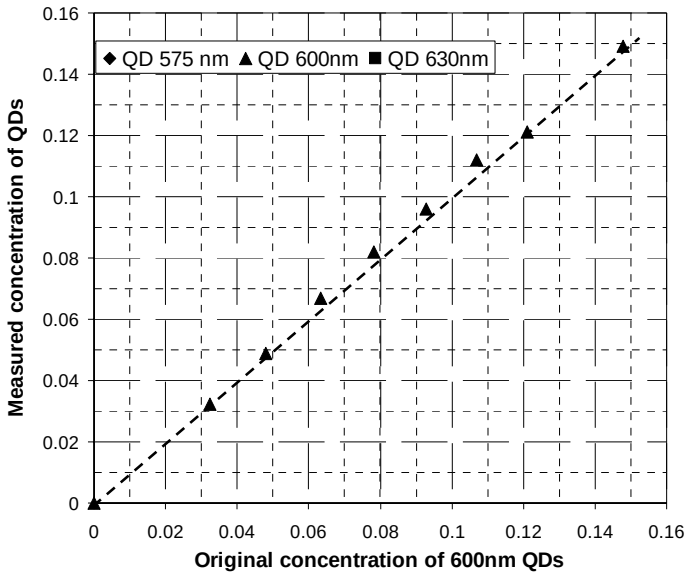

Figure 4.19 Concentration of QD 600nm determined experimentally versus concentration of this dye in the prepared dye mixtures.

As can be seen from Figure 4.18, the concentration of the 600nm QDs determined from the fluorescence measurements is practically equal to the original concentration of this dye in the prepared dye mixtures.

Figure 4.19 presents distribution of concentration of the 600nm QDs recovered from multiple measurements of the dye mixtures with 0.1s and 0.02s integration times.

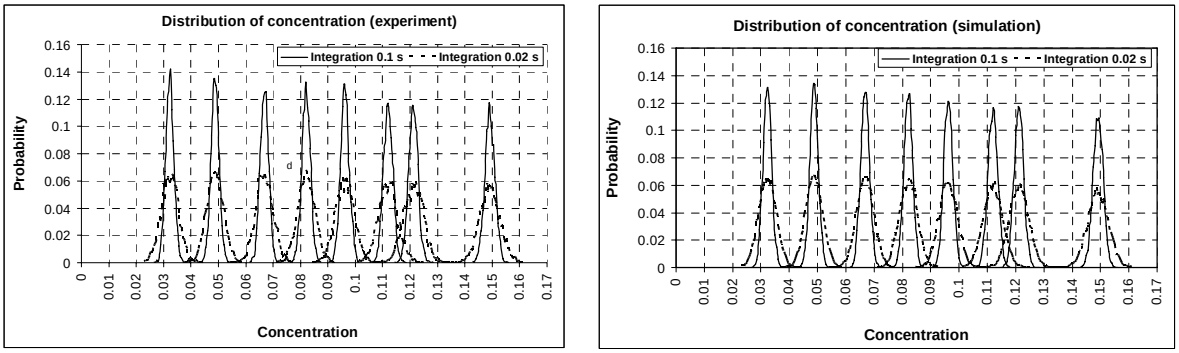

Figure 4.20 Distributions of concentrations of 600nm QD determined with 0.1s and 0.02s integration times (experiment-left panel, and simulation-right panel).

As can be seen, increase of the integration time improves the resolution of dye mixtures. Comparison of distributions of dye compositions obtained experimentally and in by the simulation shows an extremely good agreement. Based on this we conclude that the developed simulation tool can be used for prediction of the accuracy in detection and recognition of dye mixtures.

CONCLUSION

We have developed a universal fiberized single photon sensitive spectrometer based on 32-channel PMT sensor and a method for highly accurate and experimental determination of composition of mixtures containing multiple fluorescent components with overlapping spectra. The spectrometer fully satisfy the goal we set in the beginning: linearity hold up to 60-70 million counts per second without additional correction and up to 100 million counts per second with ~20% count loss, which can be corrected by post-processing.

Comparison between Monte-Carlo simulated and actual experiments results have demonstrated excellent agreement between them, which supports other evidences that our detector counts strictly follow Poisson distribution. Another conclusion we deduced from the experiments is the device non-linear output and deviation of Poisson distribution happens simultaneously.

We believe that due to an extremely high sensitivity of the photon detection in conjunction with the method for highly accurate color decomposition, the developed spectrometer may be very useful for detection and decoding of multiple color codes and it can be used in various applications which require highly accurate identification of biological samples labeled with multiple quantum dots.

BIBLIOGRAPHY

[1]. Nicewarner-Pena, S. R.; Freeman, R. G.; Reiss, B. D.; He, L.; Pena, D. J.; Walton, I. D.; Cromer, R.; Keating, C. D.; Natan, M. J. "Submicrometer metallic barcodes," Science 2001, 294, 137-141.

2. Dejneka, M. J.; Streltsov, A.; Pal, S.; Frutos, A. G.; Powell, C. L.; Yost, K.; Yuen, P. K.; Muller, U.; Lahiri, J. "Rare earth-doped glass microbarcodes," Proc. Natl. Acad. Sci. U.S.A. 2003, 100, 389-393.

[3]. Grondahl, L.; Battersby, B. J.; Bryant, D.; Trau, M. "Encoding Combinatorial Libraries: A Novel. Application of Fluorescent Silica Colloids," Langmuir 2000, 16, 9709-9715.

[4]. Braeckmans, K.; de Smedt, S.; Roelant, C.; Leblans, M.; Pauwels, R.; Demeester, J. Nat., "Encoding microcarriers by spatial selective photobleaching," Mater. (2003), 2, 169-193.

[5]. Mulvaney, S. P.; Musick, M. D.; Keating, C. D.; Natan, M. J., "Glass-coated, analyte-tagged nanoparticles: A new tagging system based on detection with surface-enhanced Raman scattering," Langmuir 2003, 19, 4784-4790.

[6]. Gao, X.; Nie, S., „Doping Mesoporous Materials with Multicolor Quantum Dots" *J. Phys. Chem. B*, 2003, *107* (42), pp 11575–11578

[7]. Ful, A., Gu, W.; Larabell, C.; Alivisatos, A.P. "Semiconductor nanocrystals for biological imaging"; Current Opinion in Neurobiology 2005, 15:568–575

[8]. Gao X., Nie S., "QD-encoded mesoporous beads with high brightness and uniformity: rapid readout by flow cytometry" Analytical Chemistry 2004,76, 2406-2410.

[9]. L. Alaverdian, S. Alaverdian, O. Bilenko, I. Bogdanov, E. Filippova, D. Gavrilov, B. Gorbovitski, M. Gouzman, G. Gudkov, S. Domratchev, O. Kosobokova, N. Lifshitz, S. Luryi, V. Ruskovoloshin, A. Stepukhovich, M. Tcherevishnick, G. Tyshko, V. Gorfinkel, "A family of novel DNA sequencing instruments based on single photon detection" Electrophoresis 23, pp. 2804-2817, 2002.

[10]. A. Tsupryk, I. Tovkach, D. Gavrilov, O. Kosobokova, G. Gudkov, G. Tyshko, B. Gorbovitski and V. Gorfinkel, "Ultra sensitive sensor with enhanced dynamic range for high speed detection of multi-color fluorescence radiation," Biosensors and Bioelectronics Volume: 23, Issue: 10, Pages: 1512-1518